# Regulation of melastatin, a TRP-related protein, through interaction with a cytoplasmic isoform

**X.-Z. Shawn Xu*†, Fabian Moebius*‡, Donald L. Gill§, and Craig Montell*¶**

*Departments of Biological Chemistry and Neuroscience, The Johns Hopkins University School of Medicine, Baltimore, MD 21205; and §Department of Biochemistry and Molecular Biology, University of Maryland School of Medicine, Baltimore, MD 21201

Communicated by M. Daniel Lane, The Johns Hopkins University School of Medicine, Baltimore, MD, July 16, 2001 (received for review June 1, 2001)

**The TRP (transient receptor potential) superfamily includes a group of subfamilies of channel-like proteins mediating a multitude of physiological signaling processes. The TRP-melastatin (TRPM) subfamily includes the putative tumor suppressor melastatin (MLSN) and is a poorly characterized group of TRP-related proteins. Here, we describe the identification and characterization of an additional TRPM protein TRPM4. We reveal that TRPM4 and MLSN each mediate $Ca^{2+}$ entry when expressed in HEK293 cells. Furthermore, we demonstrate that a short form of MLSN (MLSN-S) interacts directly with and suppresses the activity of full-length MLSN (MLSN-L). This suppression seems to result from the inhibition of translocation of MLSN-L to the plasma membrane. We propose that control of translocation through interaction between MLSN-S and MLSN-L represents a mode for regulating ion channel activity.**

The transient receptor potential (TRP) superfamily of $Ca^{2+}$-permeable cation channels includes a diverse group of channel-like proteins that resemble the prototype *Drosophila* TRP channel (1–4). Members of the TRP superfamily function in processes ranging from vasorelaxation (5) to phototransduction (6), thermal hyperalgesia (7, 8), mechanosensation (9, 10), and the acrosomal reaction and osmosensation (11–13). Among the six subfamilies of TRP proteins, the three with the greatest structural and sequence homology to *Drosophila* TRP are TRP-classic (TRPC), TRP-vanilloid (TRPV), and TRP-melastatin (TRPM) (3). Whereas most members of the first two subfamilies have been expressed and functionally characterized, the majority of TRPM proteins have not.

Members of the TRPM subfamily share ≈20% amino acid identity with TRP over a 325-aa segment that includes the C-terminal five transmembrane domains and a highly conserved 25-residue TRP domain (3). The founding member of the TRPM subfamily, melastatin (MLSN), is encoded by a gene that was isolated in a screen for genes that were down-regulated in mouse melanoma tumor-cell lines. As such, it has been suggested to be a tumor-suppressor gene (14, 15). The expression of MLSN inversely correlates with the severity of the melanocystic tumors isolated from patients (16). Moreover, treatment of melanoma cells with an agent that induces differentiation and reduces features associated with metastatic melanomas greatly potentiates MLSN expression (17). A recent study of patients with localized malignant melanomas indicates that down-regulation of MLSN RNA is a prognostic marker for metastasis (18). MLSN is alternatively spliced, and one of the major isoforms is predicted to encode a short protein (MLSN-S) that includes only the N-terminal segment but not any transmembrane domain (17). Consequently, MLSN-S would be incapable of functioning independently as an ion channel.

Two other TRPM proteins have been described that map to chromosomal positions associated with human diseases or that display alterations in expression levels in tumor cells. One such protein, MTR1, maps to a region on chromosome 11 associated with Beckwith–Wiedemann syndrome and several neoplasms (19, 20). TRP-p8 is a prostate-enriched gene that is up-regulated in a variety of tumors. The *gon-2* gene in *Caenorhabditis elegans* encodes a TRPM protein, and mutations in this locus delay or eliminate mitotic divisions of gonadal precursor cells (21). Despite the potential importance of each of these TRPM proteins, and despite the fact that they share channel-like structural motifs with the TRP superfamily, no expression studies have been undertaken to examine their cellular function or the mode by which these putative channels are regulated.

Recently, two unusual members of the TRPM family have been shown to consist of TRP channel domains fused to C-terminal enzyme domains. One such protein, TRPC7, is a candidate gene for several diseases, including bipolar affective disorder and nonsyndromic hereditary deafness (22). This protein is referred to here as "TRPM2," because "TRPC7" is also used to designate a TRPC subfamily protein (23). Interestingly, TRPM2 includes an ADP-ribose pyrophosphatase domain and seems to be activated by ADP-ribose (24). Another protein, TRP-PLIK (also LTRPC7), contains a C-terminal serine/threonine kinase domain (25). According to one report, TRP-PLIK requires protein kinase activity for channel function. However, another study does not invoke a requirement for the kinase domain for channel activity. Rather, TRP-PLIK may be regulated by $Mg^{2+}$-ATP (26). Given that none of the other TRPM proteins have been functionally expressed, the question arises as to whether those TRPM proteins lacking a C-terminal enzyme domain are ion channels capable of functioning in the absence of a regulatory C-terminal enzyme domain.

In the current work, we functionally expressed two members of the TRPM subfamily, MLSN and a previously undescribed TRPM protein, TRPM4. Each of these proteins lacks a linked enzyme domain, and yet each protein mediates cation influx in HEK293 cells. Moreover, we determined that MLSN-S, which lacks the channel-forming transmembrane domains, interacts directly with MLSN-L and suppresses the functional channel activity of the full-length form (MLSN-L) by inhibiting its translocation to the plasma membrane. We propose that the interaction between MLSN-S and MLSN-L provides a mechanism for regulating channel activity.

## Experimental Procedures

**Cloning of TRPM4.** The expressed sequence tag clone H18835, encoding a fragment of TRPM4, was used to screen human brain, placenta, and testis cDNA libraries. Several positive clones were recovered, including a 4.0-kb cDNA encoding a predicted protein of 1,040 aa. The TRPM4 cDNA was subcloned into the

Abbreviations: GST, glutathione *S*-transferase; GFP, green fluorescent protein; MLSN, melastatin; MLSN-L, full-length MLSN; MLSN-S, short form of MLSN; TRP, transient receptor potential; TRPC, TRP-classic; TRPM, TRP-melastatin; YFP, yellow fluorescent protein.

Data deposition: The sequence reported in this article has been deposited in the GenBank database (accession no. AY046396).

†Present address: Division of Biology 156-29, California Institute of Technology, Pasadena, CA 91125.

‡Present address: Institut für Biochemische Pharmakologie, Peter Mayr Strasse 1, A-6020 Innsbruck, Austria.

¶To whom reprint requests should be addressed. E-mail: cmontell@jhmi.edu.

The publication costs of this article were defrayed in part by page charge payment. This article must therefore be hereby marked "*advertisement*" in accordance with 18 U.S.C. §1734 solely to indicate this fact.



www.pnas.org/cgi/doi/10.1073/pnas.191360198

vector pcDNA3 (Invitrogen) to create pTRPM4. The coding region was fused to an N-terminal FLAG tag.

**Construction of MLSN Clones.** The coding regions of the human cDNAs encoding MLSN-L (1,533 aa) and MLSN-S (500 aa) were fused to N-terminal MYC tags and subcloned in pcDNA3 to create pcDNA3-hMLSN and pcDNA3-N-MLSN-500, respectively.

**RNA Blot Analyses.** Multiple-tissue RNA blots (CLONTECH) were probed according to standard procedures with a $^{32}$P-labeled 1.5-kb fragment generated from the 3′ end of the TRPM4 cDNA. The fetal RNA was pooled from various developmental stages (9–26 weeks).

**Transfections and $Ca^{2+}$ Imaging.** Transfections of HEK293 cells were performed with Lipofectamine (BRL) according to the manufacturer's instructions. A plasmid encoding yellow fluorescent protein (YFP) was cotransfected at ≤1/15 of the total DNA. The ratio of pMLSN-S and pMLSN-L DNA used for the transfections was 2:1. The cells were replated on coverslips coated with polylysine 24 hr after transfection, and the $Ca^{2+}$ imaging experiments were performed 12–24 hr later.

The 340- and 380-nm images were acquired with a cooled charge-coupled device camera (CoolSNAPfx, Roper Scientific, Trenton, NJ) and processed with RATIOTOOL software (Inovision, Raleigh, NC). Cells were loaded with 5 μM fura-2-AM (Calbiochem) at 37°C for 30 min in a $Ca^{2+}$-containing solution (140 mM NaCl, pH 7.4/1.2 mM $MgCl_2$/2.5 mM $CaCl_2$/10 mM glucose/14 mM Hepes/4 mM KCl). After the fura-2-AM solution had been removed, cells were maintained in the $Ca^{2+}$ solution until the experiments were initiated. To select cells for the analyses, fields were randomly chosen before the UV light was turned on. All YFP-positive cells in a randomly chosen field (typically 10–20 cells) were selected for data collection. Individual traces selected for display (Figs. 3 *E* and *F* and 4 *A* and *B*) were similar to the average trace in a given experiment.

The $Ca^{2+}$-free solution was identical to the $Ca^{2+}$ solution except that 2.5 mM EGTA was substituted for the $Ca^{2+}$. The $Sr^{2+}$- or $Ba^{2+}$-containing solutions were prepared by adding 5 mM $SrCl_2$ or $BaCl_2$ to the $Ca^{2+}$-free solution. To prepare the hypotonic solution (hOs), the $Ca^{2+}$ solution was diluted 33% with $H_2O$, and additional $CaCl_2$ was added to maintain the $Ca^{2+}$ concentration at 2.5 mM. Sucrose (10%) was added to the $Ca^{2+}$-containing solution to generate the hypertonic solution.

**Immunofluorescence.** A plasmid encoding green fluorescent protein (GFP) was cotransfected in HEK293 cells at ≤1/15 of the total DNA. Cells were replated on polylysine-coated coverslips 24 hr after transfection and incubated for ≈12 hr at 37°C. Cells were fixed with 3.7% (vol/vol) formaldehyde in PBS. The cells then were permeabilized in PBS containing 0.5% Triton X-100, blocked in PBS containing 2% (vol/vol) newborn goat serum and 1% BSA, incubated with the primary antibodies, and then incubated with the secondary antibodies. The confocal images were acquired with an Oz confocal laser scanning microscope (Noran Instruments, Middleton, WI) and processed for three-dimensional deconvolution. To select cells for analyses, one investigator performed the immunostainings and a second investigator, who was unaware of the plasmids used for the transfections, selected and photographed random fields. All of the stainings were repeated at least three times.

**Glutathione *S*-Transferase (GST) Pull-Down Assays.** The cDNA encoding MLSN-S was inserted in pGEX-KG and the GST-MLSN-S fusion protein was expressed in *Escherichia coli* (BL-21) by induction with isopropyl β-D-thiogalactoside. The fusion protein or GST alone was purified with glutathione beads, as described by the manufacturer (Amersham Pharmacia), by taking advantage of the specific affinity of GST for glutathione. The purified GST-MLSN-S (0.5 μg) or GST (1 μg) was immobilized on glutathione beads (25 μl) and incubated with MLSN-L or MLSN-S translated *in vitro* with [$^{35}$S]methionine (10 μl, Promega) in TBST [20 mM Tris/150 mM NaCl/0.5% Triton X-100 containing protease inhibitors (Roche Molecular Biochemicals), pH 7.5] for 1.5 hr. After three washes, the bound beads were eluted with SDS sample buffer, and the eluates were fractionated by SDS/PAGE followed by autoradiography.

## Results

**TRPM4, a Member of the TRPM Family.** To identify new members of the TRPM family, we scanned the Expressed Sequence Tags database (at http://www.ncbi.nlm.nih.gov/dbEST/) and identified a human cDNA clone (H18835) that included a 105-aa deduced sequence that exhibited significant homology to known TRPM proteins. Subsequently, we screened several human cDNA libraries and isolated a cDNA encoding a predicted protein of 1040 aa with six putative transmembrane domains (Fig. 1). We refer to this protein as TRPM4 (TRP-MLSN-4) because it displays a high level of sequence identity (≈30–40%) to members of the TRPM subfamily over nearly the entire protein. Within the TRPM subfamily, TRPM4 was most related to MTR1 and least similar to TRP-p8 (Fig. 2*A*). As is the case with other TRPM proteins, TRPM4 displayed ≈20% identity to members of the TRPC subfamily over a 325-aa region that included the C-terminal five transmembrane segments and the TRP domain.

The *TRPM4* RNA was expressed in most adult tissues, but at the highest levels in the heart, prostate, and colon (Fig. 2*B*). No transcripts were detected in leukocytes. In the fetus, *TRPM4* RNA was most abundant in the kidneys. There were at least two distinct bands detected on the Northern blot (6.2 kb and 4.2 kb), indicating alternative splicing of *TRPM4*. In addition to the two major RNA species, a much smaller but relatively abundant 2.4-kb RNA was detected in the testes (Fig. 2*B*). Examination of the Human Genome database (at http://www.ncbi.nlm.nih.gov/genome/guide/human) indicates that the *TRPM4* gene maps to 19q13.32. Two human diseases map to this position: orofacial cleft-3 and autosomal dominant spastic paraplegia.

**TRPM4 Mediates $Ca^{2+}$ Entry.** To determine whether the expressed TRPM4 protein may have $Ca^{2+}$ channel properties, we transiently expressed TRPM4 in HEK293 cells and undertook protein localization studies as well as fura-2 ratiometric $Ca^{2+}$-imaging analyses. To identify successfully transfected cells, we cotransfected cells with pTRPM4 and pYFP. The TRPM4 protein was localized very close to the plasma membrane, as indicated by confocal microscopy (Fig. 3 *A* and *B*).

We found that transient expression of TRPM4 increased $Ca^{2+}$ entry activity in HEK293 cells. Cells expressing YFP (Fig. 3*C*; top three traces) typically had a higher basal concentration of $Ca^{2+}$ than nontransfected cells (Fig. 3*C*; bottom trace). Moreover, removal of $Ca^{2+}$ from the bath solution triggered a decrease in $Ca^{2+}$ in the YFP-positive cells but not in the nontransfected cells (Fig. 3*C*) or in the control cells cotransfected with the empty pcDNA3 vector and pYFP (Fig. 3*D*). Reintroduction of $Ca^{2+}$ to the bath solution resulted in rapid $Ca^{2+}$ entry in most of the cells cotransfected with pTRPM4 and pYFP (72% ± 4%, $n$ = 180). The nonresponding cells (28%) may represent cells that did not express TRPM4 or expressed TRPM4 at very low levels. After $Ca^{2+}$ entry, the $Ca^{2+}$ concentration in the pTRPM4-transfected cells transiently rose above the basal $Ca^{2+}$ level, suggesting that TRPM4 may undergo $Ca^{2+}$ feedback regulation. No such entry of $Ca^{2+}$ was observed in nontransfected cells (Fig. 3*C*, bottom trace) or in transfected control cells (Fig. 3*D*).


**Fig. 1.** Alignment of TRPM4 with other TRPM proteins. Shown are the sequences corresponding to TRPM4, MTR1, TRPM2 (formerly TRPC7), MLSN-L (MLSN), and TRP-PLIK (TRPPK). The alignment was generated with CLUSTALX. To maximize the alignment, several gaps, indicated by the dashes, were introduced. The sequences corresponding to several small regions in MLSN and TRP-PLIK are not shown. The numbers of residues not shown are indicated at the appropriate positions. The positions of the six putative transmembrane segments (S1–6) and the TRP domain are indicated. The sizes of the C-terminal sequences not shown in MTR1, TRPM2, MLSN, and TRP-PLIK are indicated. Amino acids that are identical in at least two sequences are indicated with a black box. If a second pair of amino acids is conserved at the same position, it is indicated by the shading in gray. The running tally of amino acids is indicated to the left.

To characterize the TRPM4-dependent influx further, we tested the effects of cations that inhibit or permeate known channels within the TRP superfamily. The TRPM4-mediated $Ca^{2+}$ entry was rapidly blocked by 80 $\mu$M $La^{3+}$ (Fig. 3*E*, $n = 38$) as well as by 80 $\mu$M $Gd^{3+}$ (data not shown). When $Sr^{2+}$ rather than $Ca^{2+}$ was present in the bath solution, there was no change

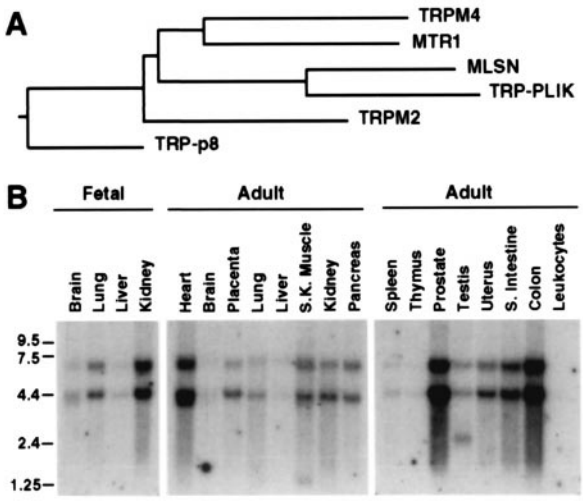


**Fig. 2.** TRPM4 is a member of the TRPM subfamily. (*A*) Phylogenetic tree. The tree was generated with the MEGALIGN software (DNAStar) after assembling the alignment with CLUSTALX. (*B*) Tissue distribution of TRPM4 RNA. Fetal and adult multiple-tissue RNA blots were probed with a labeled TRPM4 cDNA. RNA size markers (in kb) are shown.

in fluorescence, indicating that the TRPM4 channels were impermeable to $Sr^{2+}$ (Fig. 3*F*, $n = 25$). $Ba^{2+}$ entered the cells efficiently (Fig. 3*F*, $n = 25$), although the high level of $Ba^{2+}$

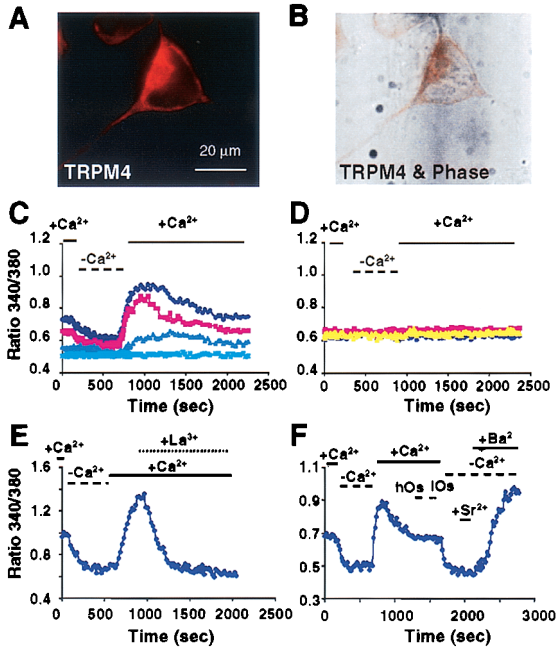


**Fig. 3.** Expression of TRPM4 promotes $Ca^{2+}$ influx. (*A*) Confocal image of TRPM4 localization in HEK293 cells. The TRPM4 protein was detected with antibodies that recognize the N-terminal FLAG epitope tag. (*B*) The immunofluorescent image in *A* was superimposed on the phase-contrast image acquired from the same cell. (*C*) TRPM4-expressing cells exhibited an increase in $Ca^{2+}$ influx. HEK293 cells were cotransfected with pTRPM4 and pYFP. After incubation with fura-2-AM, the YFP-positive cells were selected for $Ca^{2+}$ imaging. The bottom trace was a YFP-negative cell. $Ca^{2+}$-containing and $Ca^{2+}$-free solutions were changed as indicated. (*D*) Control cells transfected with an empty pcDNA3 vector and pYFP. (*E*) The TRPM4-dependent $Ca^{2+}$-influx activity was sensitive to 80 $\mu$M $La^{3+}$. (*F*) Expression of TRPM4 led to an influx of $Ba^{2+}$ but not $Sr^{3+}$. Application of solutions with high and low osmolarity (hOs and lOs, respectively) had no effect on $Ca^{2+}$ influx.

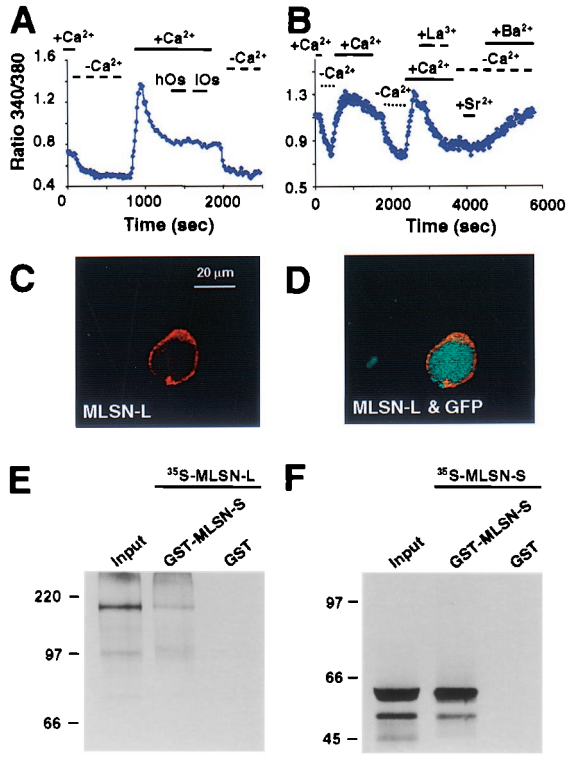


**Fig. 4.** Activity, spatial localization, and protein interactions of MLSN-L. (*A*) Expression of MLSN-L increased $Ca^{2+}$ influx in HEK293 cells. Cells were cotransfected with pMLSN-L and pYFP; $Ca^{2+}$ influx was assessed by $Ca^{2+}$ imaging. (*B*) MLSN-L was sensitive to $La^{3+}$ (80 $\mu$M) inhibition and promoted the influx of $Ba^{2+}$ but not $Sr^{2+}$. (*C*) Confocal image of the MLSN-L protein. Cells were cotransfected with pMLSN-L (MYC tagged) and pGFP and stained with anti-MYC antibodies. (*D*) The spatial distribution of GFP (green) was superimposed on the confocal image of MLSN-L (same cell as in *C*). (*E*) MLSN-L interacted with MLSN-S in pull-down assays. A GST-MLSN-S fusion protein or GST alone was bound to glutathione beads and incubated with MLSN-L labeled *in vitro* with [$^{35}$S]methionine. The beads were washed, and bound proteins were eluted with SDS sample buffer and fractionated by SDS/PAGE. The input lanes (*E* and *F*) contain 10% of the probes used in the experiments. (*F*) MLSN-S formed homomeric interactions. A $^{35}$S-labeled MLSN-S probe was incubated with GST-MSLN-S or GST alone immobilized on glutathione beads. The beads were washed and the eluted proteins were fractionated by SDS/PAGE. Protein size markers (in kDa) are shown.

accumulation is, in part, caused by the inability of pumps to remove $Ba^{2+}$ from the cytosol. Nontransfected cells did not exhibit $Ba^{2+}$ influx over a similar time scale; however, low levels of $Ba^{2+}$ influx were detected after ≈50 min (data not shown). Unlike some TRPV proteins, TRPM4 did not respond to alterations in osmolarity (Fig. 3*F*, $n = 25$). These data indicate that TRPM4 is able to function as a divalent cation channel with a specificity for ions of $Ca^{2+} \geq Ba^{2+} \gg Sr^{2+}$.

**MLSN Is a Plasma Membrane Protein Mediating $Ca^{2+}$ Entry.** To obtain additional evidence that members of the TRPM subfamily promote cation influx, we expressed the founding member of the TRPM subfamily, MLSN, in HEK293 cells and performed $Ca^{2+}$ imaging. Expression of MLSN in these cells led to a pronounced $Ca^{2+}$ entry upon switching the cells from the $Ca^{2+}$-free to the $Ca^{2+}$-containing solution; however, alterations in osmolarity had no effect (Fig. 4*A*, $n = 280$). Nontransfected cells or cells cotransfected with pYFP and the empty pcDNA3 vector did not display changes in $Ca^{2+}$ concentration upon switching from the $Ca^{2+}$-free to the $Ca^{2+}$-containing bath solutions (Fig. 3*D*). As was the case with TRPM4, $Ca^{2+}$ entry mediated by MLSN was

CELL BIOLOGY

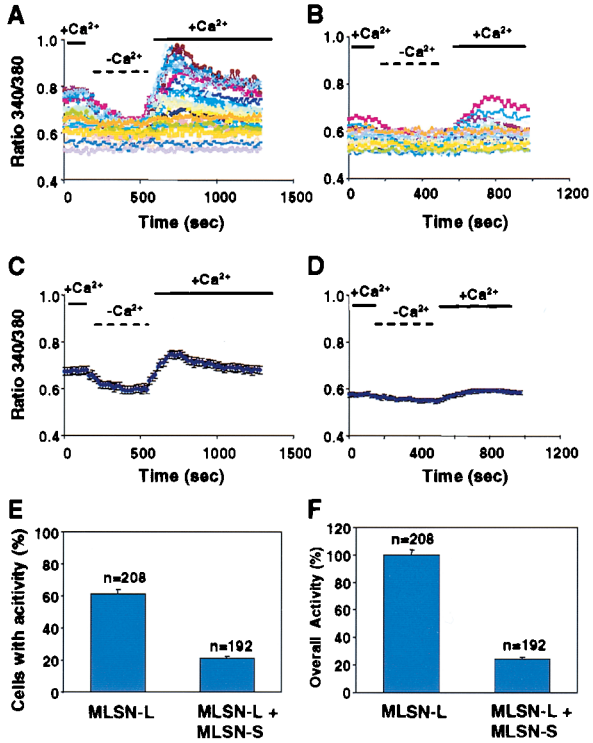


**Fig. 5.** MLSN-S suppressed the activity of MLSN-L. (*A*) $Ca^{2+}$-influx activity in MLSN-L-expressing cells. A typical experiment in which 12 of 21 cells displayed $Ca^{2+}$-entry activity is shown. (*B*) Suppression of MLSN-L activity by MLSN-S. Shown is a typical experiment in which a lower ratio (5 of 20) of cells coexpressing MLSN-L and MLSN-S displayed $Ca^{2+}$-entry activity than cells expressing MLSN-L alone. The average 340/380 ratio was also lower in those cells that exhibited $Ca^{2+}$ influx. (*C*) Average 340/380 ratios obtained from the traces shown in *A*. (*D*) Average 340/380 ratios obtained from the traces shown in *B*. (*E*) A lower percentage of cells cotransfected with MLSN-L and MLSN-S showed $Ca^{2+}$-influx activity than cells transfected with MLSN-L alone. Those cells that displayed an increase in the 340/380 ratio of $\geq$0.05 after reapplication of $Ca^{2+}$ were scored as displaying a positive response. (*F*) The overall level of MLSN-L-dependent $Ca^{2+}$-influx activity was suppressed by MLSN-S. The $Ca^{2+}$-influx activity was calculated as follows for each individual cell: the 340/380 ratio in the $Ca^{2+}$-free solution was subtracted from the peak 340/380 ratio after $Ca^{2+}$ reapplication. The average value obtained from those cells expressing MLSN-L alone was defined as 100%. In *C–F*, error bars represent SEM.

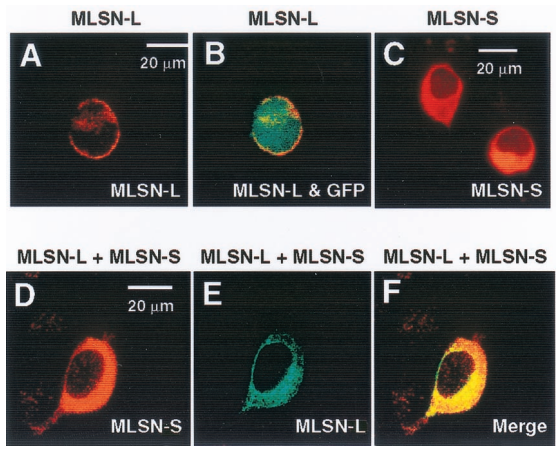


**Fig. 6.** MLSN-S altered the subcellular localization of MLSN-L. The spatial distributions of MLSN-L and MLSN-S were examined with confocal microscopy. (*A*) MLSN-L was primarily localized in or near the plasma membrane. HEK293 cells expressing MYC-tagged MLSN-L were stained with anti-MYC antibodies. (*B*) Relative spatial distributions of GFP and MLSN-L. Image of the anti-MYC staining (cell shown in *A*) is merged with the GFP localization. (*C*) MLSN-S was detected mainly in the cytosol. Cells expressing FLAG-tagged MLSN-S were stained with anti-FLAG antibodies. (*D–F*) Cells cotransfected with pMLSN-L (MYC tagged) and pMLSN-S (FLAG tagged) were double stained with rabbit anti-MYC and mouse anti-FLAG antibodies. The images were acquired with confocal microscopy. (*D*) Staining pattern for MLSN-S in cells expressing both MLSN-L and MLSN-S. (*E*) Localization of MLSN-L in cells expressing MLSN-L and MLSN-S. (*F*) The merged image of the staining patterns shown in *D* and *E*.

blocked by $La^{3+}$. There was no $Sr^{2+}$ permeation, and $Ba^{2+}$ entry was considerably slower than $Ca^{2+}$ entry (Fig. 4*B*, $n = 32$), indicating that MLSN channels have a divalent cation selectivity with $Ca^{2+} > Ba^{2+} \gg Sr^{2+}$. To determine the subcellular localization of MLSN, we performed immunofluorescent microscopy on transfected HEK293 cells. The confocal images indicated that the MLSN protein was localized at or in close proximity to the plasma membrane (Fig. 4 *C* and *D*).

**Direct Protein Interaction Between MLSN Isoforms.** MLSN is alternatively spliced, resulting in the production of a long form (MLSN-L; 1533 residues; ref. 15) and a short, N-terminal form devoid of any putative transmembrane segments [MLSN-S; 542 residues in the mouse (14) and 500 residues in humans (17)]. Whereas expression of MLSN-L promoted $Ca^{2+}$ influx (Fig. 4 *A* and *B*), introduction of MLSN-S in HEK293 cells did not (data not shown). We considered the possibility that this short isoform may play a regulatory role. To test this possibility, we first examined whether MLSN-S could directly interact with MLSN-L by performing *in vitro* pull-down assays. We found that $^{35}S$-labeled MLSN-L interacted with GST-MLSN-S but not with GST (Fig. 4*E*). MLSN-S interacted strongly with itself as $^{35}S$-labeled MLSN-S bound efficiently to GST-MLSN-S (Fig. 4*F*). MLSN-S and MLSN-L also coimmunoprecipitated after expressing the proteins *in vitro* (data not shown).

**MLSN-S Suppresses the Activity of MLSN-L.** The observation that MLSN-S interacted directly with MLSN-L raised the possibility that MLSN-S may regulate the activity of MLSN-L. Therefore, we tested the functional consequences of coexpressing MLSN-S and MLSN-L in HEK293 cells. We found that introduction of MLSN-S along with MLSN-L significantly suppressed the MLSN-L-dependent $Ca^{2+}$ entry (Fig. 5). The percentage of cells exhibiting $Ca^{2+}$-influx activity was reduced by 65.5% [from 61% $\pm$ 3% ($n = 208$) to 21% $\pm$ 1% ($n = 192$), Fig. 5*E*] and the overall $Ca^{2+}$-influx activity was suppressed by 75.5% (Fig. 5*F*). In addition to the reduction in the level of $Ca^{2+}$ influx, those cells coexpressing MLSN-S and MLSN-L displayed a longer lag between introduction of $Ca^{2+}$ to the bath solution and production of the peak levels of intracellular $Ca^{2+}$ (162 sec to 288 sec; Fig. 5 *C* and *D*).

**MLSN-S Alters the Localization of MLSN-L.** Having identified an inhibitory effect of MLSN-S on MLSN-L activity, we attempted to explore its underlying molecular mechanism. One possibility was that MLSN-S could potentially block transport of MLSN-L to the plasma membrane. To test this hypothesis, we compared the spatial distribution of MLSN-L in the presence and absence of MLSN-S. Expression of just MLSN-L resulted in a localization juxtaposed to or in the plasma membrane (Fig. 4 *C* and *D* and Fig. 6 *A* and *B*). Introduction of MLSN-S alone in HEK293 cells resulted in a cytosolic-staining pattern (Fig. 6*C*). Strikingly, upon coexpression of MLSN-S with MLSN-L, we found that MLSN-L was no longer enriched in the plasma membrane. Instead, MLSN-L was detected primarily in the cytosol and displayed a spatial distribution that overlapped extensively, but not completely, with MLSN-S (Fig. 6 *D–F*). Whereas MLSN-S appeared

to be uniformly distributed in the cytoplasm, the spatial distribution of MLSN-L had a more punctate appearance.

## Discussion

Members of the TRPM family are candidate proteins for involvement in several types of human disease. However, functional characterization of TRPM family members has been limited. In this article, we demonstrate that expression of either TRPM4 or MLSN in HEK293 cells elicited $Ca^{2+}$ influx, indicating that these members of the TRPM subfamily function as $Ca^{2+}$-permeable channels.

*MLSN* is expressed in melanocytes and has been described as a tumor suppressor that may regulate the metastatic potential of melanomas (14, 16). However, it is unclear how reduction of MLSN function may promote metastasis. Our observation that MLSN mediates $Ca^{2+}$ entry suggests a role for $Ca^{2+}$ in regulating the metastatic potential of melanomas.

Although the properties of the MLSN and TRPM4-dependent cation entry are not identical, they seemed to be similar. Expression of either of these proteins promoted entry of $Ca^{2+}$ and $Ba^{2+}$, but not $Sr^{2+}$. Moreover, the channels (when expressed) seemed to be at least partially opened and subject to a negative feedback effect by $Ca^{2+}$. The $Ca^{2+}$ influx mediated by either of these two proteins was inhibited by either 80 $\mu$M $La^{3+}$ or 80 $\mu$M $Gd^{3+}$. Thus, MLSN and TRPM4 seemed to function autonomously as cation channels, although neither of these proteins included a linked enzyme domain like TRP-PLIK and TRPM2 (TRPC7).

Given that neither MLSN nor TRPM4 contains a regulatory enzyme domain, we attempted to identify an alternative process that might regulate these TRPM proteins. The observation that one of the major *MLSN* RNAs encodes an isoform, MLSN-S, that is devoid of predicted transmembrane domains and channel activity, prompted us to speculate that MLSN-S might regulate the activity of MLSN-L. Consistent with this proposal, we found that MLSN-S interacted directly with MLSN-L. The interaction seemed to occur through the N terminus of MLSN-L because MLSN-S, which consists of the N-terminal 500 residues of MLSN-L, can also form homomeric interactions. The *Drosophila* TRPC proteins TRP, TRP-like (TRPL), and TRP$\gamma$ also interact in various pairwise combinations through their N termini (27, 28). However, the N termini of TRPM and TRPC proteins do not display sequence homology. In further support for a regulatory role for MLSN-S, we found that coexpression of the two proteins interfered with transport of MLSN-L to the plasma membrane. Consequently, there was a reduction in the activity of MLSN-L.

We suggest that the function of MLSN-S is to regulate transport of MLSN-L to the plasma membrane. According to this model, MLSN-L is retained in intracellular compartments through association with MLSN-S under basal conditions. Upon stimulation of the relevant as-yet-unidentified signaling pathway, MLSN-S is then released, thereby permitting transport of MLSN-L to the plasma membrane, thus permitting $Ca^{2+}$ entry. Retention of MLSN-L in an intracellular compartment may be the critical mode regulating $Ca^{2+}$ influx, as localization of MLSN-L in the plasma membrane leads to constitutive $Ca^{2+}$ influx.

Alternative splicing also occurs with other TRPM members. In the case of MTR1, an alternatively spliced isoform encodes a shorter protein, which is unlikely to possess channel activity because it truncates the last two transmembrane segments and the entire C-terminal domain (20). The short form of MTR1 includes the highly conserved N-terminal portion that mediates channel interaction in MLSN. Thus, it is possible that this alternatively spliced MTR1 isoform may also play a regulatory role. Although we do not know the structure of the protein encoded by the testis-specific 2.4-kb transcript of TRPM4, it would be predicted to be considerably shorter than the TRPM4 protein characterized in this article and could potentially serve a regulatory role as well. We suggest that interactions between alternative isoforms and retention in the cytoplasm may be a common mechanism for regulating the activity of those TRP proteins that form constitutively active influx channels.

We thank V. Setaluri for providing the cDNAs encoding MLSN-S and MLSN-L. F.M. was supported by Human Frontier Science Program Fellowship LT0518/1998-M. This work was supported by Grant EY10852 from the National Eye Institute (to C.M.).



1. Harteneck, C., Plant, T. D. & Schültz, G. (2000) *Trends Neurosci.* **23,** 159–166.
2. Montell, C. & Rubin, G. M. (1989) *Neuron* **2,** 1313–1323.
3. Montell, C. (2001) *Science's STKE*, http://stke.sciencemag.org/cgi/content/full/OC_sigtrans;2001/90/re1.
4. Hardie, R. C. & Minke, B. (1992) *Neuron* **8,** 643–651.
5. Freichel, M., Suh, S. H., Pfeifer, A., Schweig, U., Trost, C., Weissgerber, P., Biel, M., Philipp, S., Freise, D., Droogmans, G., *et al*. (2001) *Nat. Cell Biol.* **3,** 121–127.
6. Montell, C. (1999) *Annu. Rev. Cell Dev. Biol.* **15,** 231–268.
7. Davis, J. B., Gray, J., Gunthorpe, M. J., Hatcher, J. P., Davey, P. T., Overend, P., Harries, M. H., Latcham, J., Clapham, C., Atkinson, K., *et al*. (2000) *Nature (London)* **405,** 183–187.
8. Caterina, M. J., Leffler, A., Malmberg, A. B., Martin, W. J., Trafton, J., Petersen-Zeitz, K. R., Koltzenburg, M., Basbaum, A. I. & Julius, D. (2000) *Science* **288,** 306–313.
9. Colbert, H. A., Smith, T. L. & Bargmann, C. I. (1997) *J. Neurosci.* **17,** 8259–8269.
10. Walker, R. G., Willingham, A. T. & Zuker, C. S. (2000) *Science* **287,** 2229–2234.
11. Strotmann, R., Harteneck, C., Nunnenmacher, K., Schultz, G. & Plant, T. D. (2000) *Nat. Cell Biol.* **2,** 695–702.
12. Liedtke, W., Choe, Y., Marti-Renom, M. A., Bell, A. M., Denis, C. S., Sali, A., Hudspeth, A. J., Friedman, J. M. & Heller, S. (2000) *Cell* **103,** 525–535.
13. Wissenbach, U., Bödding, M., Freichel, M. & Flockerzi, V. (2000) *FEBS Lett.* **485,** 127–134.
14. Duncan, L. M., Deeds, J., Hunter, J., Shao, J., Holmgren, L. M., Woolf, E. A., Tepper, R. I. & Shyjan, A. W. (1998) *Cancer Res.* **58,** 1515–1520.
15. Hunter, J. J., Shao, J., Smutko, J. S., Dussault, B. J., Nagle, D. L., Woolf, E. A., Holmgren, L. M., Moore, K. J. & Shyjan, A. W. (1998) *Genomics* **54,** 116–123.
16. Deeds, J., Cronin, F. & Duncan, L. M. (2000) *Hum. Pathol.* **31,** 1346–1356.
17. Fang, D. & Setaluri, V. (2000) *Biochem. Biophys. Res. Commun.* **279,** 53–61.
18. Duncan, L. M., Deeds, J., Cronin, F. E., Donovan, M., Sober, A. J., Kauffman, M. & McCarthy, J. J. (2001) *J. Clin. Oncol.* **19,** 568–576.
19. Enklaar, T., Esswein, M., Oswald, M., Hilbert, K., Winterpacht, A., Higgins, M., Zabel, B. & Prawitt, D. (2000) *Genomics* **67,** 179–187.
20. Prawitt, D., Enklaar, T., Klemm, G., Gärtner, B., Spangenberg, C., Winterpacht, A., Higgins, M., Pelletier, J. & Zabel, B. (2000) *Hum. Mol. Genet.* **9,** 203–216.
21. West, R. J., Sun, A. Y., Church, D. L. & Lambie, E. J. (2001) *Gene* **266,** 103–110.
22. Nagamine, K., Kudoh, J., Minoshima, S., Kawasaki, K., Asakawa, S., Ito, F. & Shimizu, N. (1998) *Genomics* **54,** 124–131.
23. Okada, T., Inoue, R., Yamazaki, K., Maeda, A., Kurosaki, T., Yamakuni, T., Tanaka, I., Shimizu, S., Ikenaka, K., Imoto, K. & Mori, Y. (1999) *J. Biol. Chem.* **274,** 27359–27370.
24. Perraud, A. L., Fleig, A., Dunn, C. A., Bagley, L. A., Launay, P., Schmitz, C., Stokes, A. J., Zhu, Q., Bessman, M. J., Penner, R., *et al*. (2001) *Nature (London)* **411,** 595–599.
25. Runnels, L. W., Yue, L. & Clapham, D. E. (2001) *Science* **291,** 1043–1047.
26. Nadler, M. J., Hermosura, M. C., Inabe, K., Perraud, A. L., Zhu, Q., Stokes, A. J., Kurosaki, T., Kinet, J. P., Penner, R., Scharenberg, A. M. & Fleig, A. (2001) *Nature (London)* **411,** 590–595.
27. Xu, X.-Z. S., Li, H.-S., Guggino, W. B. & Montell, C. (1997) *Cell* **89,** 1155–1164.
28. Xu, X. Z., Chien, F., Butler, A., Salkoff, L. & Montell, C. (2000) *Neuron* **26,** 647–657.